A Four-Level Inverter Fed Open-End Winding Induction Motor Drive for Sugarcane Shredder in Sugar Industry

Vinay Kumar, *Member, IEEE*, and Sanjiv Kumar, *Senior Member, IEEE*

***Abstract*—This article presents a four-level inverter fed open-end winding induction motor drive, consisting of coupled motors, for the sugarcane shredding machine of the sugar industry. In the existing two-level inverter-fed variable frequency drive, there are drawbacks such as high harmonic distortions in the input current and inverter output voltage, high common mode voltage, and higher dV/dt stress on inverter switches. The proposed drive addresses these issues with the existing drive. The drive is an 18-pulse ac–dc converter and four-level inverter-based drive with reduced hardware components in comparison to the existing popular topologies for the four-level inverter. Experimental studies are carried out through a prototype and using OPAL-RT as a controller. The simulation is carried out on MATLAB/Simulink platform and the results are validated through the experimental results to check its efficacy for the application in sugar industry.**

***Index Terms*—Four-level inverter, load balance, open-end winding induction motor (OEWIM), shredder, volt/hertz.**

I. Introduction

THE machines used for shredding sugarcane, which is also known as shredder, is a highly inertial dual motor driven machine in the sugar industry [1], [2]. Besides the sugar industry, nowadays, dual or multimotor drives are very common in several other industrial applications, such as cement, automotive, and other industries that require multiple independently controlled electric motors [3], [4], [5], [6]. The dual motor drive system offers better reliability and other industry-specific advantages [7], [8]. As the shredder demands a high starting torque, therefore, conventionally, slip ring induction motors (SRIMs) are used as prime movers for these machines [9]. These motors are switched through their rotor circuit by inserting suitable resistances and in other industries, in general, the entire resistance is cut off in steps through contactors after achieving the preset speed [10]. But in the particular application in the sugar industry, a part of the resistance, the value of which is such that it offers up to 15% slip at full load, is kept in line throughout the operation making these drives highly inefficient due to high slip power loss [11]. Recently, the basic 2-level inverter-based variable frequency drives (VFDs) for coupled squirrel cage induction motors (IMs) have been implemented in some of the factories, for the application, with the usual configuration of one VFD for each motor. It has a standard arrangement of ac–dc conversion with delta/star-delta ($\angle 0°/\angle 30°$, $\angle 0°$) type three winding isolation transformer and two 6-pulse rectifiers connected to each one of the secondary windings making overall configuration as 12-pulse ac–dc converter [11], [12]. The VFD run IM drives have proved to be better than the conventional drives in many aspects of sugar industry [13], [14]. However, it has demerits of high harmonic distortions (in both the input current and the inverter output voltage), high dV/dt stress over the inverter switches and common mode voltage (CMV) [15], [16]. A dual inverter fed open-end winding induction motor (OEWIM) drive is a promising alternative as it can address the issues, to a large extent, with the existing VFDs feeding star or delta wound IMs. Such drives have been widely studied, implemented in various industrial applications, and presented in the literature during the last few years [17], [18], [19]. The dual inverter fed OEWIM has been reported to use either two dc supplies as in [20] or a single dc supply as in [21].

In this article, an 18-pulse ac–dc converter and four-level inverter-fed coupled OEWIM drive is presented for a sugarcane shredder. The block diagram of the drive is shown in Fig. 1 and it is novel to the sugar industry. The drive for the application

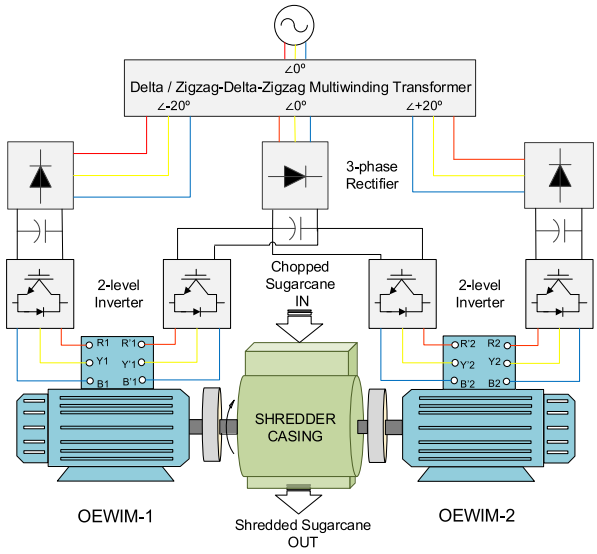

Fig. 1. Block diagram of the proposed OEWIM drive.

Manuscript received 27 July 2023; revised 29 November 2023 and 28 January 2024; accepted 18 March 2024. Date of publication 27 March 2024; date of current version 16 May 2024. Recommended for publication by Associate Editor D. Zhang. *(Corresponding author: Vinay Kumar.)*

The authors are with the Department of Electrical Engineering, Harcourt Butler Technical University, Kanpur 208002, India (e-mail: vinay_ind@yahoo.com; sanjiv.iitr@gmail.com).

Color versions of one or more figures in this article are available at https://doi.org/10.1109/TPEL.2024.3381794.

Digital Object Identifier 10.1109/TPEL.2024.3381794

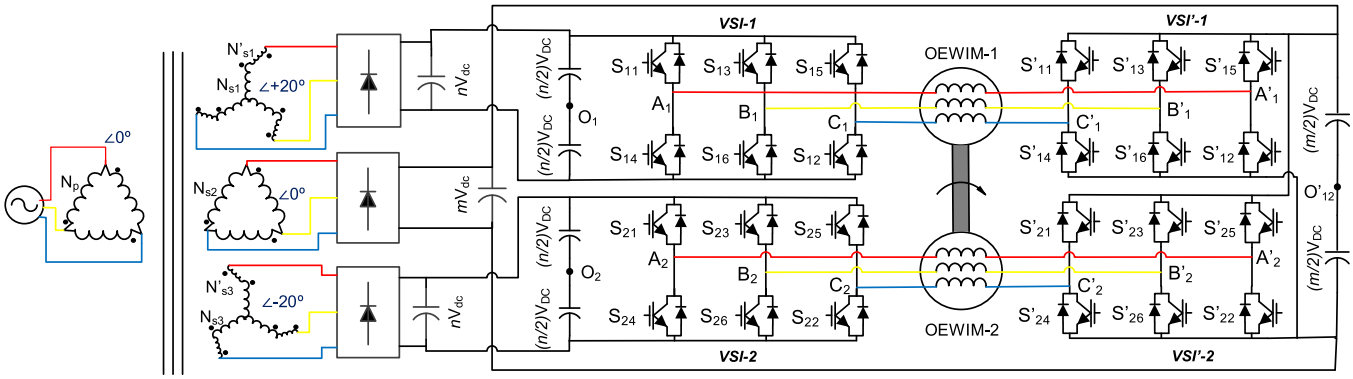

Fig. 2. Power circuit of the proposed drive.

comes under the low-dynamics category for which open-loop volt/hertz control would have been an obvious choice. But, due to a huge variation in the load, the speed is subjected to change by a large step, therefore, the open-loop would easily become unstable [22]. Hence, for the present experiment, the scalar (volt/hertz) closed-loop control method is used. In the experiment, the OPAL-RT platform is used as a controller. Simulation is carried out on the MATLAB/Simulink platform assuming the coupling to be rigid. A prototype is developed and experimental results are obtained to validate the simulation results. The load to the coupled motors is realized by using a spring balance-belt pulley-braking disc system.

II. Power Circuit of the Proposed Drive and the Inverter Output Voltage Levels

A. Power Circuit

Fig. 2 shows the power circuit diagram for the proposed drive. For the input dc voltage to the four inverters, three isolated dc sources are used making it an 18-pulse ac–dc converter. The 18 or higher pulse converters are reported to meet recommended standards for harmonics, for the input current, without any filters [23], provided, the load current is equal in each set of individual three 6-pulse ac–dc converters. For such converters, a phase-shift transformer or a multipulse rectifier is required. A phase shift type isolation transformer is used in the proposed drive. The use of an isolation step-down transformer is also relevant as each of the OEWIM drives needs one-third and two-thirds of its rated voltage for its operation.

A zero sequence current circulates in the motor windings when a common dc source is used for the two inverters feeding an OEWIM, which results in machine overheating, increasing system losses, and causing the torque ripple [18]. Further, due to the CMV, the bearing current and the failure of the motor bearing are other problems seen in such drives [24]. An appropriate modulation strategy for the inverters such as reported in [25] or using isolated dc sources, as reported in [26], can address the issues. In the proposed drive, three isolated dc sources are used and are incorporated using a multiwinding isolation transformer having delta/zigzag-delta-zigzag ($\angle 0°/+\angle 20°$, $\angle 0°$, $-\angle 20°$) configuration. Fig. 3 shows the vector representations, in terms of the windings turn ratio, of phase "*A*" of the zigzag secondary winding, having $+\angle 20°$ phase shift, with respect to the phase "*A*" of the central delta secondary.

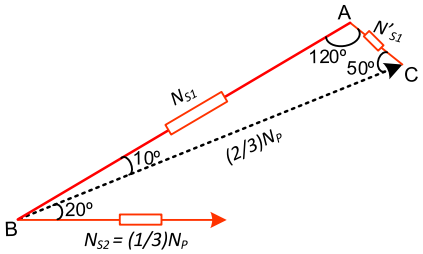

Fig. 3. Phasor diagram of central delta ($\angle 0°$) and zigzag ($+\angle 20°$) windings.

In the power circuit diagram, for $m = n$ a three-level output voltage is available and for $m \neq n$, a four-level output voltage can be obtained [27]. In the present model, for a four-level output voltage, the values of m and n are taken as 1/3 and 2/3, respectively. To get the required dc-link voltage, the turn ratio for different windings of the multiwinding transformer is given in the following equation:

$$N_p : N_{s1} : N'_{s1} : N_{s2} : N_{s3} : N'_{s3} = 1 : (2/3)x : (2/3)y : 1/3 : (2/3)x : (2/3)y \,. \quad (1)$$

The value of "x" and "y" in (1) is computed by applying the Law of Sines in ΔABC (see Fig. 3) and is evaluated to be as $x = 0.885$ and $y = 0.201$. For a multiwinding transformer, the VA rating can be estimated as half times the sum of the product of voltage across each winding and the current through them [28]. Considering this, the transformer rating for the proposed drive is taken as 3.5 kVA.

B. Inverter Output Voltage and CMV

1) Dual Inverter Output Voltage Levels: For the dc–ac conversion, an OEWIM requires two inverters operating in a dual mode. In the proposed drive, as shown in Fig. 2, two two-level voltage source inverters (VSIs), viz. VSI-1 and VSI'-1 run motor-1 and VSI-2 and VSI'-2 run motor-2. The difference in the output voltage of the two inverters of each motor is used to operate it. The pole voltages, phase voltages, etc., which are defined and presented for a single OEWIM drive in [29] are also applicable to the proposed four-level OEWIM coupled drive. In the figure, the potential difference between the points A_1 and O_1 ($V_{A_1O_1}$), B_1 and O_1 ($V_{B_1O_1}$), and C_1 and O_1 ($V_{C_1O_1}$) are the pole voltages for VSI-1 and similarly, $V_{A'_1O'_{12}}$, $V_{B'_1O'_{12}}$, $V_{C'_1O'_{12}}$ are the pole voltages for VSI'-1. $V_{O_1O'_{12}}$ is the mid-point voltage difference between the two power sources. For the sake of

brevity, only one set of equations, for the OEWIM-1, is presented here and is defined in (2)–(7). All the equations can easily be obtained on the same line for the OEWIM-2 also.

Equation (2) gives the set of phase voltages of the OEWIM-1

$$\begin{aligned} V_{A_1A'_1} &= V_{A_1O_1} - V_{A'_1O'_{12}} + V_{O_1O'_{12}} \\ V_{B_1B'_1} &= V_{B_1O_1} - V_{B'_1O'_{12}} + V_{O_1O'_{12}} \\ V_{C_1C'_1} &= V_{C_1O_1} - V_{C'_1O'_{12}} + V_{O_1O'_{12}}. \end{aligned} \tag{2}$$

Assuming that the loads of three-phase windings are symmetrical, then (3) holds [30]

$$V_{A_1A'_1} + V_{B_1B'_1} + V_{C_1C'_1} = 0. \tag{3}$$

The set of difference of pole voltages for the "*A*," "*B,*" and "*C*" phases for motor-1 are expressed as follows:

$$\begin{aligned} \Delta V_{A_1A'_1} &= V_{A_1O_1} - V_{A'_1O'_{12}} \\ \Delta V_{B_1B'_1} &= V_{B_1O_1} - V_{B'_1O'_{12}} \\ \Delta V_{C_1C'_1} &= V_{C_1O_1} - V_{C'_1O'_{12}}. \end{aligned} \tag{4}$$

Taking the sum of all three equations in (2) and substituting (3) and (4) in the sum obtained, then the mid-point voltage difference between two power sources, V_{O1O12}, in terms of the difference of pole voltages, is given in the following equation, which is the same expression as for the CMV defined in [29]:

$$V_{O_1O_{12}} = \frac{1}{3}\left(\Delta V_{A_1A'_1} + \Delta V_{B_1B'_1} + \Delta V_{C_1C'_1}\right). \tag{5}$$

Substituting (5) and the equation for phase "*A*" from (4) in the equation for phase "*A*" in (2), then the phase voltage for the OEWIM-1 (phase "*A*") can be expressed in terms of the difference of pole voltages as follows:

$$V_{A_1A'_1} = \frac{2}{3}\left(\Delta V_{A_1A'_1}\right) - \frac{1}{3}\left(\Delta V_{B_1B'_1} + \Delta V_{C_1C'_1}\right). \tag{6}$$

Similarly, the other phase voltages can also be obtained. Further, the magnitude of pole voltages for phase "*A*" of OEWIM-1 can be expressed as (7), where, S_{1A_1} and $S'_{1A'_1}$ indicate switching pulse applied to the "*A*" phase of VSI-1 and VSI'-1, respectively,

$$V_{A_1O_1} = \left(\frac{n}{2}V_{\rm DC}\right) S_{1A_1};\ V_{A'_1O_{12}} = \left(\frac{m}{2}V_{\rm DC}\right) S'_{1A'_1}. \tag{7}$$

Table I gives the possible switch combinations and the levels (L-1–L-13) in the output phase voltage (phase "*A*") for the pair of inverters (VSI-1 and VSI'-1) for $m = 1/3$ and $n = 2/3$. It also shows the number of switching redundancies (shown in the bracket) for each level. For one VSI, there are eight possible combinations of switches and therefore, altogether, 64 combinations are possible for a pair of VSIs. Out of these 64 combinations resulting in vectors, 36 are called active vectors, one is a null vector [31]. Each switch can take the state of "P" or "N" with the complementary state for the switch in the same leg. In the table, "P" indicates that the upper switch in the respective leg of VSI is "ON," whereas "N" indicates that the lower switch is "'ON." There are five levels, viz. 0, $\pm V_{\rm DC}/2$ and $\pm V_{\rm DC}/6$, which are available as a difference of the pole voltages for the individual phases given by (4). As a result, thirteen levels, viz. 0, $\pm V_{\rm DC}/9$, $\pm 2V_{\rm DC}/9$, $\pm V_{\rm DC}/3$, $\pm 4V_{\rm DC}/9$, $\pm 5V_{\rm DC}/9$, and $\pm 2V_{\rm DC}/3$ are available as phase voltage for each phase of the motor as given in (6). With the same explanation, we can get the same voltage levels for OEWIM-2.

TABLE I
FEASIBLE COMBINATIONS OF SWITCHES AND VOLTAGE LEVELS FOR THE "*A*" PHASE OF OEWIM-1

VSI-1	VSI'-1	$\Delta V_{A_1V_{A'_1}}$ (4)	$V_{A_1V_{A'_1}}$ (6)	Levels (Number of redundancies)
(S_{1A_1} S_{1B_1} S_{1C_1})	($S'_{1A'_1}$ $S'_{1B'_1}$ $S'_{1C'_1}$)			
(PNN)	(NPP)	+ $V_{DC}/2$	+ $2V_{DC}/3$	L-1 (1)
(PNN)	(NNP), (NPN)	+ $V_{DC}/2$	+ $5V_{DC}/9$	L-2 (2)
(PNN)	(NNN)	+ $V_{DC}/2$	+ $4V_{DC}/9$	L-3 (4)
(PNP), (PPN)	(NPP)			
(PNN)	(PPP)	+ $V_{DC}/6$		
(PNN)	(PNP), (PPN)	+ $V_{DC}/6$	+ $V_{DC}/3$	L-4 (6)
(PNP), (PPN)	(NNP), (NPN)	+ $V_{DC}/2$		
(NNN)	(NPP)	- $V_{DC}/6$	+ $2V_{DC}/9$	L-5 (7)
(PNN)	(PNN)	+ $V_{DC}/6$		
(PNP), (PPN)	(PPP)			
(PNP), (PPN)	(NNN)	+ $V_{DC}/2$		
(PPP)	(NPP)			
(NNN)	(NNP), (NPN)	- $V_{DC}/6$	+ $V_{DC}/9$	L-6 (8)
(PNP), (PPN)	(PNP), (PPN)	+ $V_{DC}/6$		
(PPP)	(NNP), (NPN)	+ $V_{DC}/2$		
(PPP)	(NNN)	+ $V_{DC}/2$	0	L-7 (8)
(PPN), (PNP)	(PNN)	+ $V_{DC}/6$		
(PPP)	(PPP)			
(NNN)	(NNN)	- $V_{DC}/6$		
(NNP), (NPN)	(NPP)			
(NNN)	(PPP)	- $V_{DC}/2$		
(NNN)	(PPN), (PNP)	- $V_{DC}/2$	- $V_{DC}/9$	L-8 (8)
(NPN), (NNP)	(NPN), (NNP)	- $V_{DC}/6$		
(PPP)	(PPN), (PNP)	+ $V_{DC}/6$		
(NNN)	(PNN)	- $V_{DC}/2$	- $2V_{DC}/9$	L-9 (7)
(NPN), (NNP)	(PPP)			
(NPN), (NNP)	(NNN)	- $V_{DC}/6$		
(NPP)	(NPP)			
(PPP)	(PNN)	+ $V_{DC}/6$		
(NPN), (NNP)	(PPN), (PNP)	- $V_{DC}/2$	- $V_{DC}/3$	L-10 (6)
(NPP)	(NPN), (NNP)	- $V_{DC}/6$		
(NPP)	(NNN)	- $V_{DC}/6$	- $4V_{DC}/9$	L-11 (4)
(NPN), (NNP)	(PNN)	- $V_{DC}/2$		
(NPP)	(PPP)			
(NPP)	(PPN), (PNP)	- $V_{DC}/2$	- $5V_{DC}/9$	L-12 (2)
(NPP)	(PNN)	- $V_{DC}/2$	- $2V_{DC}/3$	L-13 (1)

2) Common Mode Voltage: For a standard three-phase two-level VSI the CMV may take the values of $\pm V_{\rm DC}/6$ or $\pm V_{\rm DC}/2$ depending on the selection of the states of inverter switches [32]. For a three-level inverter, realized using a dual inverter with symmetric dc sources, feeding an OEWIM, the results for CMV are extensively studied and well presented in [33] and the CMV levels for it with sinusoidal pulsewidth modulation (SPWM) are reported as 0, $\pm V_{\rm DC}/6$, $\pm V_{\rm DC}/3$, and $\pm V_{\rm DC}/2$. For the proposed four-level inverter with SPWM, realized using a dual inverter with asymmetric dc sources, feeding an OEWIM, the CMV levels are given by $\pm V_{\rm DC}/18$, $\pm V_{\rm DC}/6$, $\pm 5V_{\rm DC}/18$, $\pm 7V_{\rm DC}/18$, and $\pm V_{\rm DC}/2$. The states of inverter switches with CMV are shown in Table II. Therefore, among the above three discussed cases, during switch state changes, the CMV changes by a lowest step in case of the proposed four-level inverter than in case of the two- or three-level inverters, further, its rms value is also the lowest. To reduce the CMV further, the higher levels

TABLE II
CMV FOR DIFFERENT COMBINATIONS OF THE SWITCHES FOR THE PROPOSED FOUR-LEVEL INVERTER

VSI-1 ($S_{1A_1}\ S_{1B_1}\ S_{1C_1}$)	VSI'-1 ($S_{1A'_1}\ S_{1B'_1}\ S_{1C'_1}$)	CMV (5)
(PPP)	(PPP)	+ V_{DC}/2
(PPP)	(PNP), (PPN), (NPP)	+ 7V_{DC}/18
(PNP), (PPN), (NPP)	(PPP)	+ 5V_{DC}/18
(PPP)	(NNP), (NPN), (PPN), PNN)	
(NPP), (PNP), (PPN)	(NPP), (PNP), (PPN)	+ V_{DC}/6
(PPP)	(NNN)	
(NNP), (NPN), (PNN)	(PPP)	+ V_{DC}/18
(NPP), (PNP), (PPN)	(NNP), (NPN), (PNN)	
(PNN), (NPN), (NNP)	(PPN), (PNP), (NPP)	- V_{DC}/18
(PPN), (PNP), (NPP)	(NNN)	
(NNN)	(PPP)	- V_{DC}/6
(PNN), (NPN), (NNP)	(PNN), (NPN), (NNP)	
(NNN)	(PPN), (PNP), (NNP), (NPP)	- 5V_{DC}/18
(NPN), (NNP), (PNN)	(NNN)	
(NNN)	(NPN), (NNP), (PNN)	- 7V_{DC}/18
(NNN)	(NNN)	- V_{DC}/2

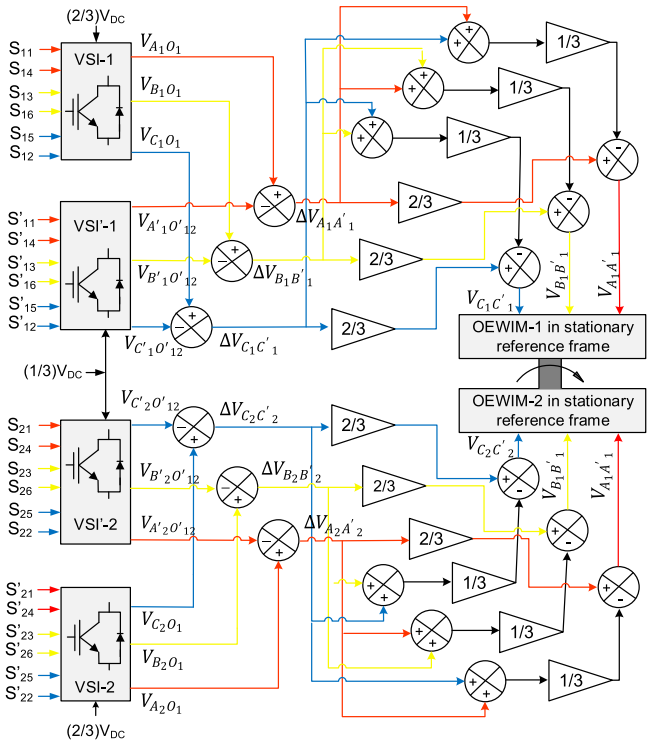

Fig. 4. Detailed discrete model of the proposed drive.

can easily be eliminated by using suitable switch combinations keeping in view the redundancies shown in Table I.

III. DISCRETE MODEL OF THE PROPOSED DRIVE

The discrete-state model is reported to be more suitable for studying inverter-fed IM control [34]. The discrete state model for an IM shall also be applicable to an OEWIM. The detailed discrete model implementation of the proposed drive is shown in Fig. 4. The various voltages (pole voltages, difference of pole voltages, and phase voltages) shown in the figure are already defined in (2)–(6).

In [35], the discrete model of OEWIM implemented in a stationary reference frame is extended for the proposed coupled OEWIMs and is given by (8)–(13) with $i = 1$ or 2 as per the motor-1 or motor-2, respectively.

The stator and rotor voltage of the motors are described in (8) and (9)

$$V_{s_i}(t) = R_{s_i} i_{s_i}(t) + \rho L_{s_i} i_{s_i}(t) \tag{8}$$

$$0 = R_{r_i} i_{r_i}(t) + \rho L_{r_i} i_{r_i}(t) - j\omega\psi_{r_i}(t). \tag{9}$$

The stator flux and rotor flux, in terms of stator and rotor currents, are given in (10) and (11):

$$\psi_{s_i}(t) = L_{s_i} i_{s_i}(t) + L_{m_i} i_{r_i}(t) \tag{10}$$

$$\psi_{r_i}(t) = L_{r_i} i_{r_i}(t) + L_{m_i} i_{s_i}(t). \tag{11}$$

By considering ψ_{si}, ψ_{ri}, and i_{si}, i_{ri} as state variables, (12) gives the torque equations for the motors and (13) gives the total torque produced by the coupled motors

$$T_i(t) = \left(\frac{3}{2}\right)\left(\frac{P}{2}\right)\left(\overrightarrow{\psi_{s_i}(t)} \times \overrightarrow{i_{r_i}(t)}\right) \tag{12}$$

$$T_{\text{total}}(t) = \left(\frac{3}{2}\right)\left(\frac{P}{2}\right)\left\{\left(\overrightarrow{\psi_{s1}(t)} \times \overrightarrow{i_{r1}(t)}\right) + \left(\overrightarrow{\psi_{s2}(t)} \times \overrightarrow{i_{r2}(t)}\right)\right\}. \tag{13}$$

In (8)–(13), R_{s_i} and R_{r_i} are the stator resistance and rotor resistance; "ρ" is the derivative (d/dt) and "P" is the number of poles. L_{s_i} and L_{r_i} are the stator inductance and rotor inductance. $\psi_{s_i}(t)$ and $\psi_{r_i}(t)$ are stator flux linkages and rotor flux linkages at the time "t." i_{s_i} and i_{r_i} are stator current and rotor current and $V_{s_i}(t)$ is stator voltage at the time "t." $T_i(t)$ is the electromagnetic torque at the time "t."

Balancing of $T_1(t)$ and $T_2(t)$ is desired in the industry, otherwise, both the motors may run with lesser efficiency as one motor shall run in overload condition and the other motor in under load condition.

IV. CONTROL STRATEGY FOR THE PROPOSED DRIVE

For the present application, the set speed may be required to be maintained for a few days as it corresponds to the condition of the hammer tips of the shredder and the variety of sugarcane, early or late. As no frequent change in the speed is required, therefore, the drive comes under a low-dynamics category application drive. Open-loop volts/hertz control is reported to be an obvious choice for such drives where high dynamic performance is not a demand [36]. The sugarcane shredding machine is subjected to an appreciable speed drop due to the frequent impact load and in such cases, the open-loop control may easily become unstable. Therefore, the open-loop control may not be suitable for the application [22]. In [37], authors have well presented the closed loop volts/hertz control using a fuzzy logic based auto-tune controller for an open-end winding machine fed by an MLI but, the control circuitry shall be rather complex and costlier for the present application. Keeping in view the requirement of a simple and suitable control strategy for the application, the closed-loop volts/hertz control with slip regulation is implemented in the proposed drive. The block diagram is shown in Fig. 5. Two dc supply of magnitude (2/3)V_{DC} each is given to the two VSIs (one from each motor drive) and another dc supply of magnitude

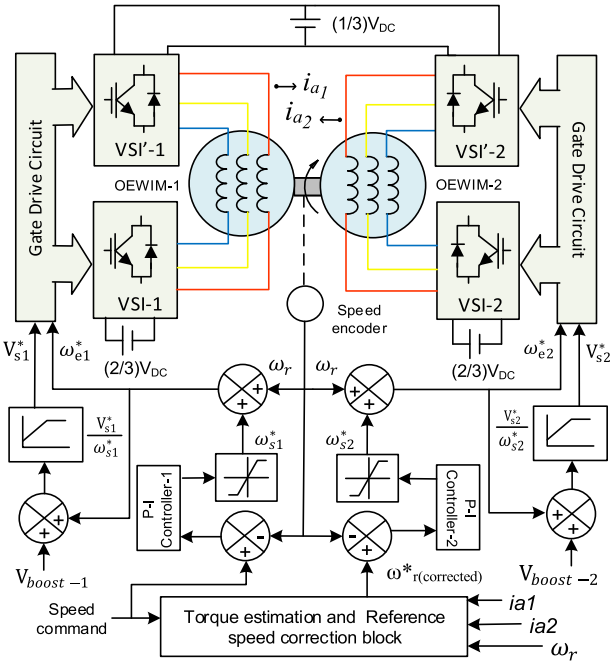

Fig. 5. Control strategy of the proposed drive.

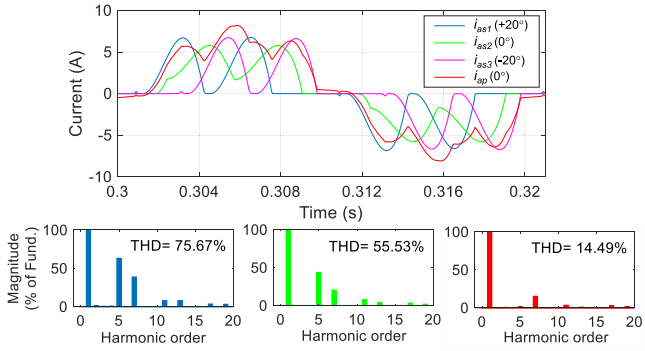

Fig. 6. Simulation results for input current and harmonic spectrum for secondary-1, secondary-2, and primary windings.

TABLE III
PARAMETERS OF EACH OEWIM

Parameter	Description	Value
R_s	Stator resistance (Ω)	12.7
R_r	Rotor resistance (Ω)	6.1 for Motor-1 7.1 for Motor-2
L_s	Stator leakage inductance (H)	0.28
L_r	Rotor leakage inductance (H)	0.12
L_m	Magnetizing inductance (H)	0.48
V_N	Rated voltage (V)	400
P	Power (kW)	1.1
J	Moment of inertia (kg·m^2)	0.015
T_N	Rated torque (N·m)	7.5
N_r	Rated speed (r/min)	1410

$(1/3)V_{\rm DC}$ is given commonly to the remaining two VSIs. The actual speed of the motor is compared with the set speed "$\omega^*{}_s$" and the error generates the slip frequency command through a proportional-integral (P-I) controller and a limiter. The slip so obtained is added to the feedback speed to generate the voltage and frequency command. The value of "K_p" and "K_i" in the P-I controllers is taken as 2 and 25, respectively.

The command signal (corresponds to the speed or frequency) and the proportional voltage signal "$V^*{}_s$" derived from it is given in the following equation:

$$V^*{}_s = \left(\frac{V_b}{\omega_b}\right)\omega_s^* \tag{14}$$

where "V_b" and "ω_b" are the base voltage and base angular frequency, respectively. The boost voltage, "$V_{\rm boost}$," is added to this signal to compensate for the stator resistance losses and to ensure flux does not decrease at low frequency [38].

For the shredding machine application in the sugar industry, the load-sharing problem has been observed to be very common, predominantly in the conventional SRIM drive. Various control strategies such as master-slave control, use of scalar control with slip and torque compensations, weighted control strategy, etc. have been reported in the literature to address the problem in other industrial applications [39], [40], [41]. For the coupled motors of the same rating, the variation in the rotor resistance is the most significant reason for variation in their torque-speed characteristics. For such a system where the motors are of the same rating but have different rotor resistance, the voltage and the frequency fed to the machine should be different. The impact of dissimilar rotor resistance can be reduced significantly and to an acceptable level by using a reference speed correction block as shown in the figure. To get the two torques to be equal at the operating point, the reference speed for OEWIM-2 (the motor with the higher rotor resistance) is taken as per the following equation:

$$\omega^*{}_{r(\rm corrected)} = \omega^*{}_r + \alpha_T\,(T_{e_1} - T_{e_2}) \tag{15}$$

where "$\omega^*{}_{r(\rm corrected)}$" is the corrected reference speed command to the OEWIM-2 and "$\omega^*{}_r$" is the reference speed for OEWIM-1. "α_T" is the torque weighing factor. The value of the torque weighing factor is empirically selected after performing several simulations. Its value is anywhere between 2.5 and 3.5 found to give a fairly good load balance.

V. SIMULATION AND EXPERIMENTAL RESULTS

The block diagram of the proposed drive as shown in Fig. 5 was implemented by using MATLAB/Simulink. The simulated results are shown in Figs. 6–9. The simulated results so obtained are verified experimentally through a prototype. In the experiment, OPAL-RT is used as a controller and also for the hardware-in-the-loop testing for the power converters. The experimental results are shown in Figs. 10–15. The various parameters of the two OEWIMs are shown in Table III. The rotor resistance of OEWIM-2 is kept deliberately higher than the rotor resistance of OEWIM-1 using rheostat to simulate load-imbalanced conditions.

A. Simulation Results

1) Results for AC–DC Conversion Stage: Fig. 6 shows the simulation results for the input current and its harmonics. In

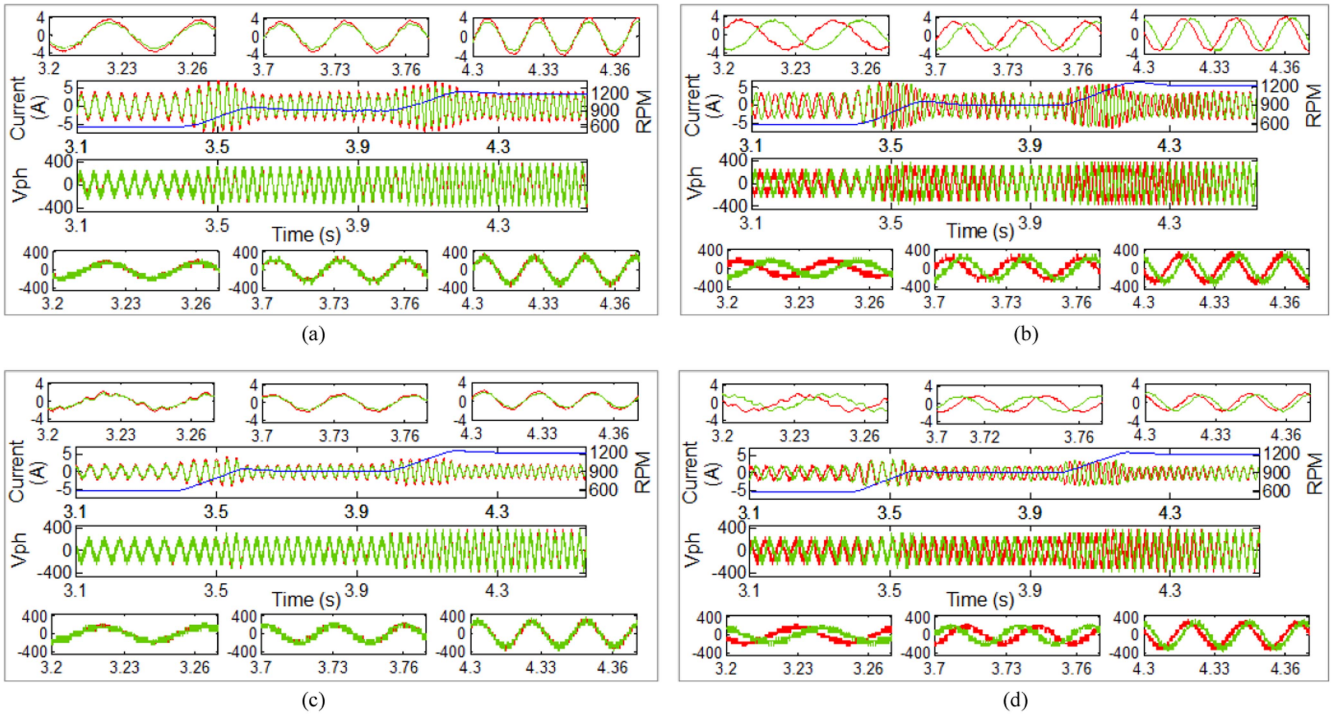

Fig. 7. Simulation results for motor current, inverter output voltage and speed. At full load—(a) without and (b) with the reference speed correction. At half load—(c) without and (d) with the reference speed correction.

the figure, the currents, "$i_{a_{s1}}$," "$i_{a_{s2}}$," "$i_{a_{s3}}$," and "i_{a_p}" are waveforms of the current in phase "*A*" of the secondary-1, 2, 3, and primary windings respectively. The harmonic spectrum for the currents, "$i_{a_{s1}}$," "$i_{a_{s2}}$," and "i_{a_p}" is also shown. The magnitude and waveform shape of "$i_{a_{s3}}$" and "$i_{a_{s1}}$" are almost same, therefore, the harmonic spectrum of "$i_{a_{s3}}$" is not presented for the sake of brevity. The currents "$i_{a_{s1}}$" and "$i_{a_{s3}}$" are observed to be in discontinuous mode, whereas "$i_{a_{s2}}$"is observed to be in continuous mode, therefore, its total harmonics distortion is also lower [42]. Also, the secondary-2 winding is feeding two VSIs through a single rectifier resulting in "$i_{a_{s3}}$" to be double of the "$i_{a_{s1}}$" or "$i_{a_{s3}}$." The current "i_{a_p}" is vector sum of the currents in the secondary windings referred to as the primary winding. Accordingly, "i_{a_p}" is given in the following equation:

$$i_{a_p} = i'_{a_{s1}} + i'_{a_{s2}} + i'_{a_{s3}} \tag{16}$$

where $i'_{a_{s1}}$, $i'_{a_{s2}}$, and $i'_{a_{s3}}$ are the phase *"A"* current in secondary windings referred to as the primary winding and are given in the following equation:

$$i'_{a_{s1}} = ni_{a_{s1}};\ i'_{a_{s2}} = mi_{a_{s2}};\ i'_{a_{s3}} = ni_{a_{s3}} \tag{17}$$

where $m = 1/3$ and $n = 2/3$. Further, by rewriting (17) in terms of the fundamental components of the currents we obtain the following equation:

$$I'_{1a_{s1}} = \left(\frac{2}{3}\right) I_{1a_{s1}};\ I'_{1a_{s2}} = \left(\frac{1}{3}\right) I_{1a_{s2}} = \left(\frac{2}{3}\right) I_{1a_{s1}} = \left(\frac{2}{3}\right) I_{1a_{s3}};\ I'_{1a_{s3}} = \left(\frac{2}{3}\right) I_{1a_{s3}}. \tag{18}$$

Therefore, though the current in the secondary-2 winding is double the current in the secondary-1 or 3 winding, the current (fundamental component) of each of the three secondary windings, when referred to as the primary winding, is equal in magnitude, giving a natural advantage to the proposed topology to get near balanced referred secondary currents in the primary winding. In the harmonic spectrum for "$i_{a_{s1}}$" as shown in the figure, among the six dominant current harmonics (5th, 7th, 11th, 13th, 17th, and 19th) the low-order dominant harmonics, viz. 5th and 7th are the most detrimental harmonics. For an 18-pulse converter, for the ideal situation of balanced current in all three secondary windings, the low-order dominant harmonics, viz. 5th, 7th, 11th, and 13th are eliminated completely [42]. In the present case, the availability of 7th- and 11th-order harmonics, but at a much-reduced magnitude, in the harmonic spectrum of "i_{a_p}" in the figure, is because the current in secondary-2 winding is continuous and, therefore, its waveform is not the same as the current in the secondary-1 and 3 windings carrying current in the discontinuous mode, even though the contribution of their fundamental components, in the primary winding current, is same as per (18). As shown, the THD for the currents, $i_{a_{s1}}$, $i_{a_{s2}}$, and i_{a_p} is observed to be 75.67%, 55.53%, and 14.49%, respectively. The THD of the input current to the transformer is seen to be reduced to a fairly good level.

2) DC–AC Conversion Stage and Load Side Results: Fig. 7 shows the simulation results for the motor current and inverter output voltage waveforms for both motors for different speed conditions (600, 900, and 1200 r/min). Fig. 7(a) and (b) shows the simulation results for the full load torque condition and Fig. 7(c) and (d) shows the results for the half load torque condition. Fig. 7(a) and (c) shows the results for the case

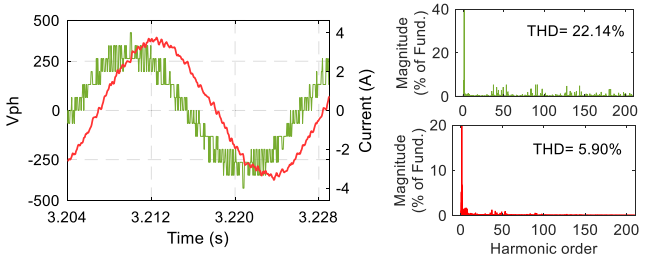

Fig. 8. Simulation results for harmonics for inverter output phase voltage and motor load current.

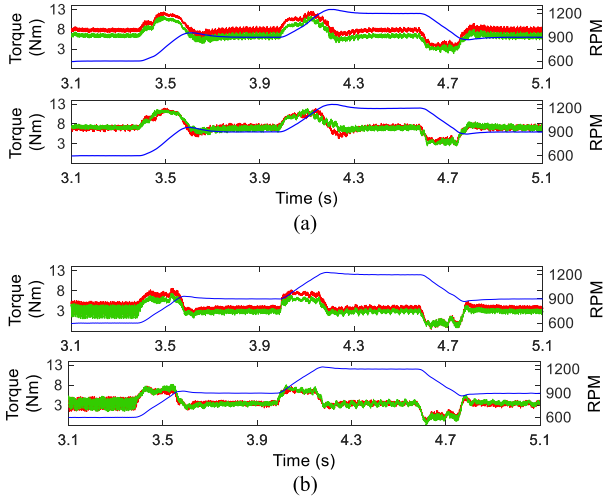

Fig. 9. Simulation results for developed torque at different speeds. (a) At full load. (b) At half load.

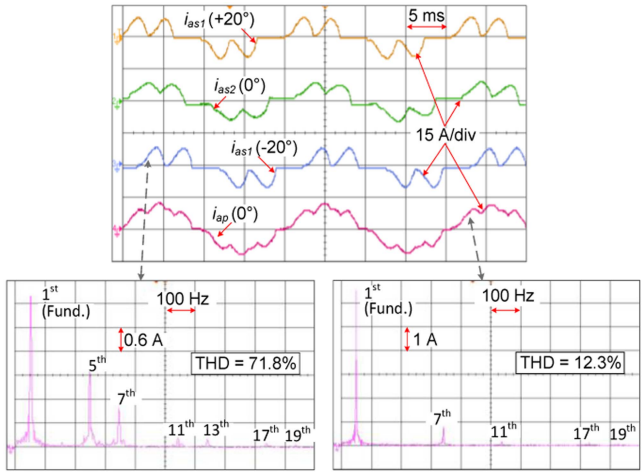

Fig. 10. Experimental results for input current waveforms and FFT for the current in secondary-3 and primary winding.

when the correction for reference speed is not implemented for motor-2 and Fig. 7(b) and (d) shows the results for the case when the proposed correction for reference speed is implemented. In Fig. 7(a) and (c), it can be seen that the inverter output voltage and its frequency remain the same for both the motor drives, the reference speed command being the same for both the drives, but, the current drawn by motor-1 is higher than that of motor-2, which is undesirable. It can also be seen that the difference in the load currents remains almost the same for all the speeds for the given load and the difference is increased for the increased load. In Fig. 7(b) and (d), it can be seen that the inverter output voltage and its frequency, being of different modulation, are different for both the motors but the load current and torque developed for the given load become equal, as desired. The phase and frequency of the two currents remained different as per the respective voltage waveform.

Fig. 8 shows the results for the harmonics for the inverter output voltage and motor current. For the sake of brevity, only one case of full load and 1200 r/min is presented. The THD for the voltage and current is obtained as 22.14% and 5.9% respectively, which is much better, being a four-level inverter-based system, than the figures for the standard two-level inverter-based systems as reported in the studies in [43] and [44]. Further, it may be seen in Fig. 7, at lower speeds, particularly at low loads, that the voltage profile attains the shape similar to a three-level inverter (having comparatively higher low-order harmonics), as a result, the current is also seen to follow the voltage. However, it is still better, even at low speeds, than the existing two-level inverter-based drive as far as the harmonics in the motor current is concerned.

Fig. 9 shows the simulation results for the torque developed at different speeds, for both the cases, i.e., without and with the implementation of correction for the reference speed. Fig. 9(a) shows the results for the full load condition and Fig. 9(b) shows the results for the half load condition. In both the respective figures, the upper figure shows the results without any correction and the lower figure shows the results when the proposed correction for the reference speed is implemented. The difference in the torques is observed to be higher for the higher loads. It can be seen that the implementation of the proposed speed reference correction block has fairly improved load sharing by the two motors.

B. Hardware Results

1) Results for AC–DC Conversion Stage: Fig. 10 shows the experimental results for the input currents, "$i_{a_{s1}}$," "$i_{a_{s2}}$," "$i_{a_{s3}}$," and "i_{a_p}" and harmonic spectrum for the currents "$i_{a_{s3}}$" and "i_{a_p}" for full load condition. During the experiment, the THD for the currents "$i_{a_{s3}}$" and "i_{a_p}" was observed to be as 71.8% and 12.3%, respectively. It can be seen that the experimental results for the input current and its harmonics fairly conform to the simulation results.

2) DC–AC Conversion Stage and Load Side Results: Figs. 11 and 12 show the experimental results obtained for the motor current drawn and inverter output voltage for different speeds (600, 900, and 1200 r/min) at full and half loads respectively. Figs. 11(a) and 12(a) show the results when no correction is provided to the reference speed for motor-2.

Figs. 11(b) and 12(b) show the results after the proposed correction for reference speed to is provided. In Figs. 11(a) and 12(a), it can be seen that the motor-1 draws more current than motor-2, which is undesirable. The voltage being equally modulated, so its waveform remains almost the same, for both motors. In Figs. 11(b) and 12(b), it can be seen that, after correction for the reference speed, the magnitude of the current

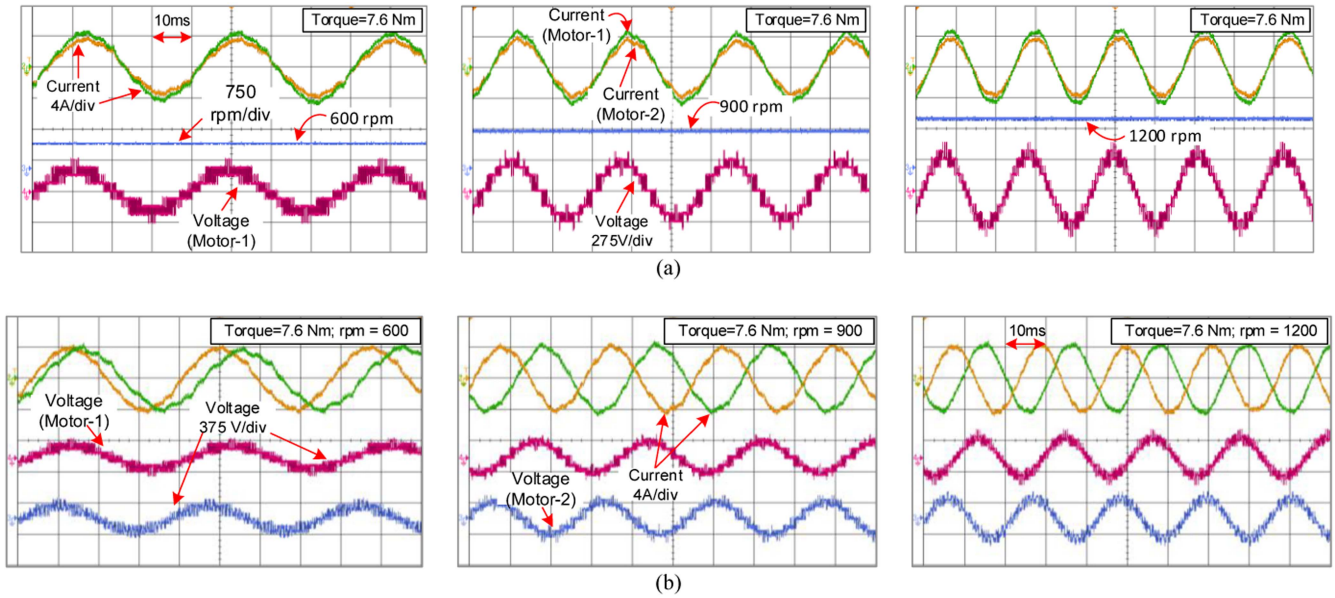

Fig. 11. Experimental results for motor current, inverter output voltage and speed for full load. (a) Without and (b) with correction for reference speed.

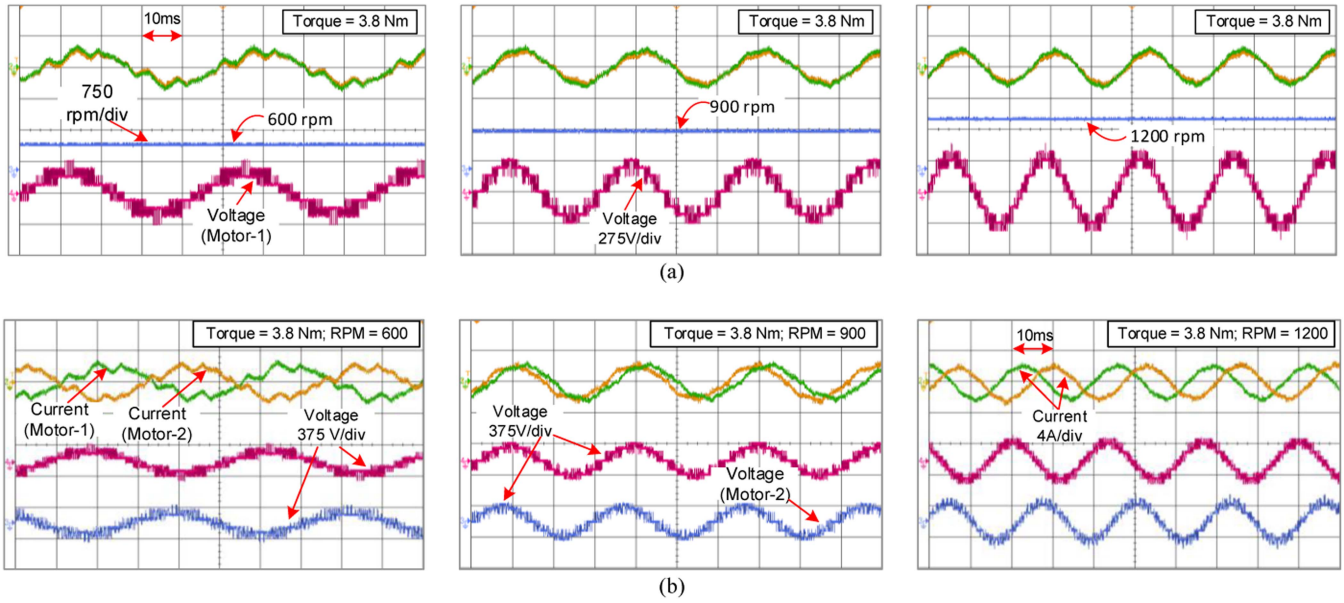

Fig. 12. Experimental results for motor current, inverter output voltage and speed for half load. (a) Without and (b) with correction for reference speed.

drawn by two motors is almost equal, as desired, and the voltage and frequency were observed to be different (which is obvious). In the figures, it can also be observed that the levels of the inverter output voltage are increasing as the speed of the motors is increased. In Figs. 11(a) and 12(a), it may also be observed that the difference in the magnitude of currents of the two motors is higher for the higher load condition.

Fig. 13 shows the experimental results for the harmonics for output voltage across motor winding and motor current for full load at a speed of 1200 r/min. The THD for the voltage and the current was found to be 24.64% and 5.2% respectively. The results obtained are fairly similar to the simulation results.

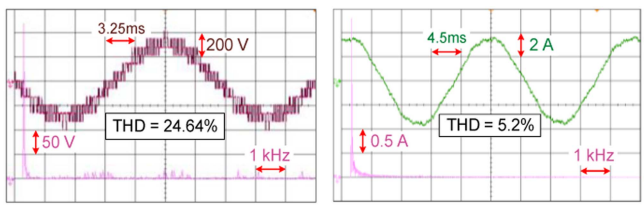

Fig. 13. Experimental results for FFT for phase voltage and motor current.

Figs. 14 and 15 show the experimental results for the set speed of 1200 and 600 r/min, respectively, for variable loads (full and half load conditions). The experimental results for

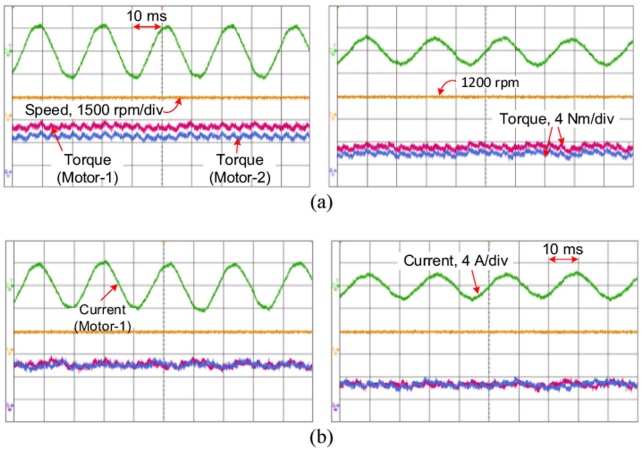

Fig. 14. Experimental results for different loads at 1200 r/min. (a) Without and (b) with correction for reference speed.

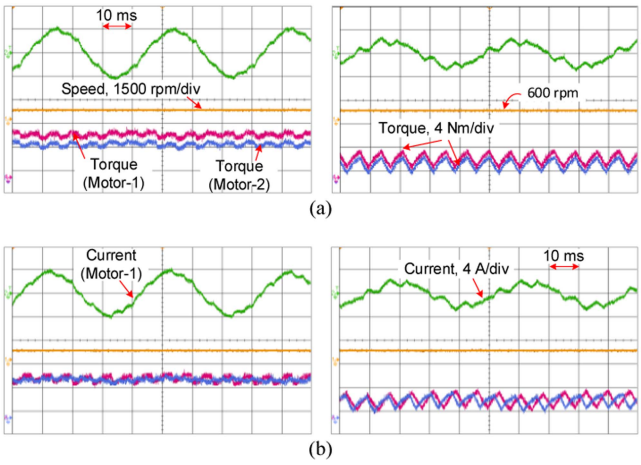

Fig. 15. Experimental results for different loads at 600 r/min. (a) Without correction for reference speed. (b) With correction for reference speed.

900 r/min are not presented for the sake of brevity. The current drawn by motor-1 is also presented to show the variation in its magnitude for different load conditions. Figs. 14(a) and 15(a) show the results for the case when no correction for the reference speed for motor-2 is provided. It can be observed that set speed is maintained for different load conditions, but motor-1 shares a higher load and develops more torque than motor-2. Figs. 14(b) and 15(b) show results for the case when the proposed correction for the reference speed for motor-2 is provided. It can be observed that both motors develop almost the same torque and hence share an equal load. It may also be observed that the difference between the torques of the two motors when no correction for the reference speed is given, is more for the higher load.

Fig. 16 shows the developed prototype and the arrangement for the experiment for implementation of the proposed drive for the sugar industry. In the ac–dc conversion section, a 3.5 kVA delta/zigzag-delta-zigzag transformer and three three-phase rectifiers are used to get isolated dc supplies and also to realize an 18-pulse ac–dc converter. The central rectifier is commonly

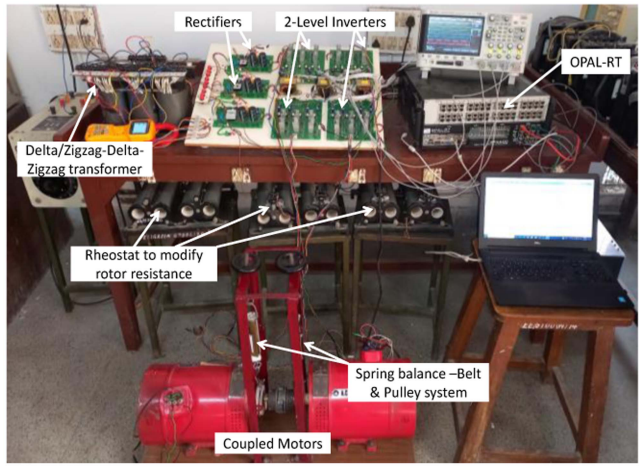

Fig. 16. Experimental setup and the prototype of the proposed drive.

TABLE IV
COMPARISON OF SOME IMPORTANT PARAMETERS

Parameters	Existing Drives		Proposed Drive
	SRIM	VFD	
THD (i/p current) [23], [46]	Not applicable	Higher (12-pulse ac–dc converter)	Lower (18-pulse ac–dc converter)
dV/dt stress and CMV [16], [32]		Higher (2-level inverter)	Lower (4-level inverter)
Overall efficiency [47], [48]	~80%	85%–90%	Slightly higher than the existing VFD
Relative cost [45]	"k" units	1.2–1.25 times "k" units	1.3–1.35 times "k" units

feeding two inverters (one from each motor drive). In the dc–ac conversion section four inverters (2-level), two each for one motor, with six IGBTs and their gate drive circuits for each inverter, are used. To obtain the currents, six ACS712 current sensors are used, one each in the "*A*" phase of the two OEWIMs and one each in the "*A*" phase of four windings of the transformer. To obtain the inverter output voltages (voltage across the "*A*" phase winding of the OEWIMs), AD202 isolation amplifier based voltage sensing circuit is used. OPAL-RT is used as a controller. Two OEWIMs (with wound rotor), each of 1.1 kW ratings are used and the rotor resistance of motor-2 is kept more than motor-1 by using rheostats.

VI. COMPARISON OF THE PROPOSED DRIVE WITH THE EXISTING DRIVES

Though a strict comparison of the proposed drive with the existing drives, viz. SRIM drive and two-level inverter-based VFD is beyond the scope of this article, but, an approximate and generalized comparison of some of the important parameters may be made based on the information in the datasheets, available literature, technical brochure, etc. of some of the reputed makes of motors and drives. The same is presented in Table IV. The mentioned overall efficiency includes the efficiencies of the transformer, motor with converters (for VFD) or rotor side starter (for SRIM). For the SRIM drives the high slip power loss in the rotor circuit has also been taken into consideration. Also, each rectifier and VSI of the proposed drive is handling one-third or two-thirds of the power of the rectifiers or VSIs of

TABLE V
HARDWARE COMPONENTS FOR A FOUR-LEVEL FC, NPC, AND PROPOSED MLI FED DUAL MOTOR DRIVES

MLI Type	No. of Switches	Clamping Diodes	Clamping Capacitors	DC Capacitors	DC supplies	DC source voltage	Pulse no.
FC	36	0	18	6	2	V_{DC}	12
NPC	36	36	0	6	2	V_{DC}	12
Proposed	24	0	0	3	3	$V_{DC}/3$ (one) and $2V_{DC}/3$ (two)	18

the existing drive, therefore, the unit-wise cost and power loss are estimated accordingly on the similar lines as presented in [45] for a three-level inverter. Further, the conventional SRIM drive does not have any power electronics devices, but, the motor is costlier than that of squirrel cage IM and OEWIM of the same rating and it also needs a rotor side starter and a step-down transformer if the bus voltage is higher than the rated voltage of the motor.

The proposed drive is also compared, for the hardware components, with the popular flying capacitor (FC) and the neutral point clamped (NPC) type MLI fed drives as defined in [49], if implemented to drive a dual motor system. The comparison is presented in Table V. The hardware components are reduced in the case of the proposed drive except for the number of dc supplies.

In comparison to the existing drives (SRIM and VFD), the cost of the proposed drive is slightly higher but it is cheaper than the other MLIs (NPC and FC) available for the four-level output voltage for having a lesser number and low rating components and also having other advantages and better efficiency as shown in Table IV. Also, though the proposed drive requires one extra dc supply (see Table V), but, it helps in mitigation harmonics in the input current, being an 18-pulse ac–dc converter.

VII. CONCLUSION

Simulation and experimental implementation of a four-level inverter-fed coupled OEWIM drive has been presented for sugarcane shredding application in the sugar industry. Both simulation and experimental results for the proposed drive have been shown. The proposed topology has a lesser number of hardware components in comparison to the other popular (FC and NPC) multilevel inverter-fed drives for the four levels and two-motor system. Therefore, comparatively, the cost is reduced for the power electronics devices for both at the ac–dc conversion stage (as only three instead of four rectifiers are used) and for realizing a four-level inverter. The load sharing has been balanced after the implementation of the reference speed correction strategy for OEWIM-2 (the motor with higher rotor resistance). A much better voltage profile with reduced CMV, in comparison to the well-known two-level inverter has been observed for the inverter output voltage and the levels were observed to be varied as per the speed and load torque demand. In this article, the emphasis is made on the introductory implementation of a four-level inverter-fed OEWIM drive for the sugar industry, with a basic SPWM technique to realize scalar (volt/hertz) closed-loop control. The future scope of the work is to extend it for more rigorous control strategies and higher level inverters, as available in the literature, for the other sections such as mills and centrifugal machines of the sugar industry, which are also having multimotor configurations and require a high dynamic performance.

REFERENCES

[1] E. Hugot, "Shredders," in *Handbook of Cane Sugar Engineering*, 3rd ed. Amsterdam, The Netherlands: Elsevier, 1986, pp. 60–72.

[2] P. Rein, *Cane Sugar Engineering*, 2nd ed. Berlin Germany: Verlas Dr. Albert Bartens KG, 2017.

[3] S. Khomfoi and L. M. Tolbert, "17 - multilevel power converters," in *Power Electronics Handbook*, M. H. Rashid, Ed., 2nd ed. New York, NY, USA: Academic, 2007, pp. 451–482.

[4] G. Seggewiss, N. Schachter, and G. Obermeyer, "Kiln drive application considerations," in *Proc. Conf. Rec. Cement Ind. Tech. Conf.*, 2005, pp. 52–76.

[5] U. R. Muduli, A. R. Beig, K. Al Jaafari, K. Al Hosani, A. S. Al-Sumaiti, and R. K. Behera, "Dual motor power sharing control for electric vehicles with battery power management," *IEEE Trans. Ind. Electron.*, vol. 70, no. 12, pp. 12024–12035, Dec. 2023.

[6] W. Cao, B. C. Mecrow, G. J. Atkinson, J. W. Bennett, and D. J. Atkinson, "Overview of electric motor technologies used for more electric aircraft (MEA)," *IEEE Trans. Ind. Electron.*, vol. 59, no. 9, pp. 3523–3531, Sep. 2012.

[7] I. G. Odnokopylov, Y. N. Dementev, I. V. Usachev, D. Y. Lyapunov, and A. S. Petrusev, "Load balancing of two-motor asynchronous electric drive," in *Proc. Int. Siberian Conf. Control Commun.*, 2015, pp. 1–4.

[8] G. Scelba et al., "Current-sharing strategies for fault-tolerant AC multidrives," *IEEE Trans. Ind. Appl.*, vol. 51, no. 5, pp. 3943–3953, Sep./Oct. 2015.

[9] D. J. Hall, "New approach to shredder drives driven by electric motors," in *Proc. South Afr. Sugar Technologists' Assoc.*, 2009, vol. 82, pp. 235–242.

[10] K. C. Agrawal, "Starting and control of slip-ring induction motors," in *Industrial Power Engineering Handbook*, 2nd ed.Oxford, U.K.: Newnes, 2007, pp. 5/81–5/96.

[11] V. Kumar and S. Kumar, "Performance comparison of electric drives for chopping/shredding sugarcane in sugar industry," *AIUB J. Sci. Eng.*, vol. 22, no. 1, pp. 14–23, 2023.

[12] J. R. Rodriguez et al., "Large current rectifiers: State of the art and future trends," *IEEE Trans. Ind. Electron.*, vol. 52, no. 3, pp. 738–746, Jun. 2005.

[13] V. Kumar and S. Kumar, "An industrial survey on electric drives and scope of multilevel inverter based induction motor drives in sugar industry," *Sugar Tech.*, vol. 23, no. 4, pp. 709–719, 2021.

[14] G. Scheuer and T. Schmager, "Medium voltage drives in the sugar industry," *Int. Sugar J.*, vol. 109, pp. 303–309, May 2007.

[15] R. Naik, T. A. Nondahl, M. J. Melfi, R. Schiferl, and J.-S. Wang, "Circuit model for shaft voltage prediction in induction motors fed by PWM-based AC drives," *IEEE Trans. Ind. Appl.*, vol. 39, no. 5, pp. 1294–1299, Sep./Oct. 2003.

[16] K. K. Gupta and P. Bhatnagar, *Multilevel Inverters: Conventional and Emerging Topologies and their Control*. U.K.: Academic, 2018.

[17] S. M. W. Ahmed, M. M. Eisa, G. M. A. Sowilam, and A. B. S. M. Salem, "Open ends induction motor operation based on a dual inverter," in *Proc. 4th Int. Des. Test Workshop*, 2009, pp. 1–6.

[18] J. Riedemann, R. Peña, and R. Blasco-Giménez, "Open-end winding induction motor drive based on indirect matrix converter," in *Induction Motors*, R. I. G. Recalde, Ed. Rijeka, Croatia: IntechOpen, 2015.

[19] S. Kumar and P. Agarwal, "Performance evaluation of 18-level inverter fed open-end winding IM drive," *IETE J. Res.*, vol. 67, no. 2, pp. 253–262, 2021.

[20] K. R. Sekhar and S. Srinivas, "Discontinuous decoupled PWMs for reduced current ripple in a dual two-level inverter fed open-end winding induction motor drive," *IEEE Trans. Power Electron.*, vol. 28, no. 5, pp. 2493–2502, May 2013.

[21] V. T. Somasekhar, K. Gopakumar, and M. Baiju, "Dual two-level inverter scheme for an open-end winding induction motor drive with a single DC power supply and improved DC bus utilisation," *IEE Proc. Electric Power Appl.*, vol. 151, pp. 230–238, 2004.

[22] B. K. Bose, *Power Electronics and Motor Drives Advances and Trends*. Amsterdam, The Netherlands: Elsevier, 2006.

[23] B. Singh, S. Gairola, B. N. Singh, A. Chandra, and K. Al-Haddad, "Multipulse AC–DC converters for improving power quality: A review," *IEEE Trans. Power Electron.*, vol. 23, no. 1, pp. 260–281, Jan. 2008.
[24] W. Hu, C. Ruan, H. Nian, and D. Sun, "Zero-sequence current suppression strategy with common-mode voltage control for open-end winding PMSM drives with common DC bus," *IEEE Trans. Ind. Electron.*, vol. 68, no. 6, pp. 4691–4702, Jun. 2021.
[25] M. R. Baiju, K. K. Mohapatra, R. S. Kanchan, and K. Gopakumar, "A dual two-level inverter scheme with common mode voltage elimination for an induction motor drive," *IEEE Trans. Power Electron.*, vol. 19, no. 3, pp. 794–805, May 2004.
[26] E. G. Shivakumar, V. T. Somasekhar, K. K. Mohapatra, K. Gopakumar, L. Umanand, and S. K. Sinha, "A multi level space phasor based PWM strategy for an open-end winding induction motor drive using two inverters with different DC link voltages," in *Proc. IEEE 4th Int. Conf. Power Electron. Drive Syst. Indonesia*, 2001, vol. 1, pp. 169–175.
[27] V. T. Somasekhar, E. G. Shivakumar, K. Gopakumar, and A. Pittet, "Multi level voltage space phasor generation for an open-end winding induction motor drive using a dual inverter scheme with asymmetrical DC-link voltages," *Eur. Power Electron. Drives J.*, vol. 12, no. 3, pp. 59–77, 2002.
[28] D. A. Paice, "Multipulse methods and transformers," in *Proc. Power Electron. Converter Harmon.: Multipulse Methods Clean Power*, 1996, pp. 25–37.
[29] K. V. P. Kumar, K. M. R. Eswar, and T. V. Kumar, "Hardware implementation of predictive torque controlled open-end winding induction motor drive with self-tuning algorithm," *Cogent Eng.*, vol. 4, no. 1, pp. 1388–3323, 2017.
[30] Y.-F. Jia, L. Chu, N. Xu, Y.-K. Li, D. Zhao, and X. Tang, "Power sharing and voltage vector distribution model of a dual inverter open-end winding motor drive system for electric vehicles," *Appl. Sci.*, vol. 8, 2018, Art. no. 254.
[31] K. V. Praveen Kumar and T. V. Kumar, "Experimental implementation of direct torque control of open end winding induction motor," in *Proc. IEEE Region Conf.*, 2016, pp. 3318–3323.
[32] A. M. Hava and E. Ün, "Performance analysis of reduced common-mode voltage PWM methods and comparison with standard PWM methods for three-phase voltage-source inverters," *IEEE Trans. Power Electron.*, vol. 24, no. 1, pp. 241–252, Jan. 2009.
[33] J. Kalaiselvi and S. Srinivas, "Bearing currents and shaft voltage reduction in dual-inverter-fed open-end winding induction motor with reduced CMV PWM methods," *IEEE Trans. Ind. Electron.*, vol. 62, no. 1, pp. 144–152, Jan. 2015.
[34] T. F. Chan and K. Shi, "Modeling and simulation of induction motor," in *Proc. Appl. Intell. Control Induction Motor Drives*, 2011, pp. 31–74.
[35] R. Krishnan, *Electric Motor Drives: Modeling, Analysis, and Control*. Englewood Cliffs, NJ, USA: Prentice Hall, 2001.
[36] J. Liu, T. A. Nondahl, P. B. Schmidt, S. Royak, and T. M. Rowan, "Generalized stability control for open-loop operation of motor drives," *IEEE Trans. Ind. Appl.*, vol. 53, no. 3, pp. 2517–2525, May/Jun. 2017.
[37] S. Kumar and P. Agarwal, "A novel FLC based closed-loop V/f control of five-level inverter fed open-end winding induction motor drive," *J. Inst. Eng., Ser. B*, vol. 100, no. 3, pp. 193–200, 2019.
[38] A. Munoz-Garcia, T. A. Lipo, and D. W. Novotny, "A new induction motor V/f control method capable of high-performance regulation at low speeds," *IEEE Trans. Ind. Appl.*, vol. 34, no. 4, pp. 813–821, Jul./Aug. 1998.
[39] D. Xiao, X. Li, and K. He, "Power balance of starting process for pipe belt conveyor based on master-slave control," *IEEE Access*, vol. 6, pp. 16924–16931, 2018.
[40] I. G. Odnokopylov, Y. N. Dementev, I. V. Usachev, D. Y. Lyapunov, and A. S. Petrusev, "Load balancing of two-motor asynchronous electric drive," in *Proc. Int. Siberian Conf. Control Commun.*, 2015, pp. 1–4.
[41] A. Bouscayrol, M. Pietrzak-David, P. Delarue, R. Peña-Eguiluz, P.-E. Vidal, and X. Kestelyn, "Weighted control of traction drives with parallel-connected AC machines," *IEEE Trans. Ind. Electron.*, vol. 53, no. 6, pp. 1799–1805, Dec. 2006.
[42] B. Wu and M. Narimani, "Multipulse diode rectifiers," in *High-Power Converters and AC Drives*. Hoboken, NJ, USA: Wiley, 2017, pp. 37–63.
[43] N. Jiao, S. Wang, and T. Liu, "Harmonic analysis of output voltage in PWM inverters," in *Proc. IEEE Int. Power Electron. Appl. Conf. Expo.*, 2018, pp. 1–5.
[44] S. Kim, Y.-D. Yoon, and S.-K. Sul, "Pulsewidth modulation method of matrix converter for reducing output current ripple," *IEEE Trans. Power Electron.*, vol. 25, no. 10, pp. 2620–2629, Oct. 2010.
[45] R. Teichmann and S. Bernet, "A comparison of three-level converters versus two-level converters for low-voltage drives, traction, and utility applications," *IEEE Trans. Ind. Appl.*, vol. 41, no. 3, pp. 855–865, May/Jun. 2005.
[46] S. Guizani, A. Nayli, and F. Ben Ammar, "Comparison between star winding and open-end winding induction machines," *Elect. Eng.*, vol. 98, no. 3, pp. 219–232, 2016.
[47] B. K. Bose, *Power Electronics and Motor Drives: Advances and Trends*. Amsterdam, The Netherlands: Elsevier, 2020.
[48] M. Schweizer, T. Friedli, and J. W. Kolar, "Comparative evaluation of advanced three-phase three-level inverter/converter topologies against two-level systems," *IEEE Trans. Ind. Electron.*, vol. 60, no. 12, pp. 5515–5527, Dec. 2013.
[49] J. Rodríguez, J.-S. Lai, and F. Z. Peng, "Multilevel inverters : A survey of topologies, controls, and applications," *IEEE Trans. Ind. Electron.*, vol. 49, no. 4, pp. 724–738, Aug. 2002.

Vinay Kumar (Member, IEEE) was born in Muzaffarnagar, U.P., India, in 1976. He received the Bachelor's degree in electrical engineering from The Institution of Engineers (India), Kolkata, India, in 2005, and the M.Tech. degree from the Visvesvaraya Technological University, Belgaum, India, in 2010. He is currently working toward the Ph.D. degree with the Department of Electrical Engineering, Harcourt Butler Technical University, Kanpur, India.

After completing his military training, he served in Indian Air Force as a combatant (technical) member from 1998 to 2011. In 2011, he joined College of Military Engineering, Government of India, Pune, India, as an Assistant Professor. In 2014, he joined the National Sugar Institute, Government of India, Kanpur, India, as an Assistant Professor (Sugar Engineering). His fields of interest include power electronics, electrical machines and drives, sugar engineering, and electric drives in sugar industry.

Mr. Kumar is a Life Member of The Institution of Engineers (India). He is also a Chartered Engineer (India).

Sanjiv Kumar (Senior Member, IEEE) was born in Kanpur, U.P., India, in 1975. He received the B.E. degree in electrical and electronics engineering from M.J.P. Rohilkhand University, Bareilly, India, in 2000, and the M.Tech. and Ph.D. degrees from the Indian Institute of Technology, Roorkee, India, in 2006 and 2016, respectively.

From 2001 to 2007, he worked in various reputed industries as an Electrical Engineer and Technical Executive. In February 2007, he joined the Department of Electrical Engineering, Harcourt Butler Technical University, Kanpur, India, as an Assistant Professor and became an Associate Professor, in 2019, and Professor, in 2022. He has authored more than 35 research papers in journals and conferences. He has delivered more than 40 invited/expert lectures in Faculty Development Programs at various institutes/colleges. His research interests include multilevel inverters, open-end winding induction motor drives, high power converters, power electronics, industrial electric drives, microprocessor control electric drives, and active power filters.

Dr. Kumar is a Fellow of Institution of Electronics and Telecommunication Engineers (IETE).